Side chain interactions in D/L peptide nanotubes. Studies by crystallography, NMR spectroscopy and molecular dynamics

Mitchell R. Silk,[a][b] Jason R. Price,[c] Biswaranjan Mohanty,[a] Hanna-Kirsti S. Leiros,[b] Bjarte A. Lund,[b] Philip E. Thompson[a] and David K. Chalmers*[a]

[a] Dr. M. R. Silk, Dr. B. Mohanty, Prof. Dr. P. E. Thompson, Dr. D. K. Chalmers
Medicinal Chemistry
Monash Institute of Pharmaceutical Sciences
Monash University
381 Royal Parade, Parkville, VIC 3052, Australia
E-mail: david.chalmers@monash.edu

[b] Dr. M. R. Silk, Prof. Dr. H.-K. S. Leiros, Dr. B. A. Lund
Department of Chemistry
UiT – The Arctic University of Norway
N-9037 Tromsø, Norway

[c] Dr. J. R. Price
Australian Synchrotron
The Australian Nuclear Science and Technology Organisation (ANSTO)
800 Blackburn Road, Clayton, VIC 3168, Australia

Supporting information for this article is given via a link at the end of the document.

Abstract: Our understanding of the factors affecting the stability of cyclic D/L peptide (CP) nanotubes remains underdeveloped. In this work, we investigate the impact of side chain alignment, hydrophobicity and charge on CP nanotube stability through X-ray crystallography, NMR spectroscopy and molecular dynamics (MD) simulations. We characterise the distinct CP-CP alignments that can form and identify stable and unstable dimers by MD simulation. We measure H-bond half-lives of synthesised CPs by ^{1}H-D exchange experiments and find good correlation with predicted CP-CP stabilities. We find that hydrophobic amino acids improve CP dimer stability but experimentally reduce solubility. Charged amino acids either increase or decrease CP dimer stability depending on the relative orientation and composition of charged groups. X-ray crystal structures are solved for two CPs, revealing non-tubular folded conformations. Ultimately, this work will assist the educated design of stable tubular structures for potential applications in biomedicine.

Introduction

Self-assembling cyclic peptides built from alternating D and L amino acids (CPs) assemble to create unique tubular, supramolecular assemblies.[1] Assembly is mediated by β-sheet-like hydrogen bonding between CP backbones.[1a, 2] The alternating chirality of the amino acids means that the side chains project outwards from the nanotube, potentially enabling control of CP nanotube (CPN) surface properties simply by modifying the amino acids in the CP sequence.[3] CP nanostructures have exciting potential applications as biomolecular mimetics, for example as pseudoproteins or artificial membrane channels.[4] However, despite the fact that CP systems have been known for more than 25 years, there have, to date, been few demonstrated applications of these systems. There has been some investigation of methods to improve our control of CPN structure and composition, particularly through covalent tethering of CPs to one-another to control the relative orientations of CP monomers in dimers,[5] and in larger heterogeneous oligomers.[6]

One of the major limitations to developing CP-based nanostructures is a lack of detailed knowledge about the factors that govern the stability of CP nanotubes. For example, there is little available information about the extent to which the incorporation of ionic or nonpolar residues influences CPN stability (**Figure 1**). Improving our structural understanding of CP nanotubes and the key factors driving self-assembly will enable us to better predict and control their assembly and ultimately enable the development functional CP-based nanomaterials.

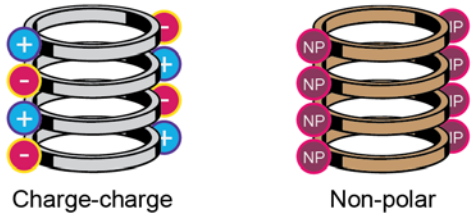

Figure 1. To what extent do side chain interactions, such as polar charge-charge interactions or non-polar hydrophobic interactions, increase nanotube stability? What role do the alignments of different side chains play in stabilising CP-CP interactions?

CP nanostructures can be investigated using a variety of techniques: crystallography, NMR and IR spectroscopy, electron microscopy or theoretically, through energy calculations or MD simulation. Crystallographic studies have investigated CPs with the backbone amides on one face blocked by methyl groups, allowing only CP dimers to form.[1b, 7] We have previously reported that CPs **1** and **2** (**Table 1**) crystallise in parallel and antiparallel nanotube forms.[9] In each case, a network of charge-charge interactions between Asp and Lys side chains reinforce the crystal lattice. CPs have also been observed to crystallise in non-tubular, folded conformations that make intramolecular backbone H-bonds rather than β-sheet-like inter-CP hydrogen bonds.[8]

NMR spectroscopy studies have also given useful insight into CP interactions. 1D ^{1}H NMR spectroscopy has been used to characterise the concentration-dependent assembly of CPs,[7a, 10] the existence of multiple CP conformations[8, 11] and to determine CP association constants.[1b, 7a, 11] Inter-CP interactions have been measured by ROESY and NOESY NMR spectroscopy, which has been used to identify the relative orientations of CPs to one-another[1b, 6b, 12] and to show the encapsulation of guest-molecules within CP cavities.[6c] The strength of H-bonding within CPN materials has been measured by 1D ^{1}H NMR spectroscopy using ^{1}H-D exchange experiments.[6a] DOSY NMR spectroscopy has been used to estimate the degree of CP aggregation in solution based on the diffusion properties of the dissolved material.[6]

Molecular dynamics (MD) simulations have been used to investigate the properties of CP nanotubes, particularly in lipid bilayers.[13] The overall structural stability of assembled CPNs was investigated by Vijayaraj *et al*., who used MD and quantum chemistry calculations to probe the effects of the number of CP subunits within a CPN. They found that CPs located at the tube termini were weakly associated, regardless of the number of subunits present and, as such, the overall stability of a CPN is determined by the length of the core-region[14] and the nature of the solvent.[15] Garcia-Fandino *et al*. used MD methods to show that α,γ-CPs can be designed to favour heterogeneous dimer assembly over homogeneous assembly. α,γ-CPs contain alternating α- and γ-amino acids rather than D-α / L-α, but achieve a flat conformation allowing the formation of similar backbone H-bonded, hollow nanotubes. *Cis*-3-aminocyclohexanecarboxylic acid (γ-Ach) and *cis*-3-aminocyclopentanecarboxylic acid (γ-Acp) incorporated into different α,γ-CPs were more stable as heterogeneous H-bonded dimers than as homodimers.[16] Liu *et al*. have studied the mechanisms behind CPN-mediated transport of the antitumor drug 5-fluorouracil, describing how the drug alternately makes hydrophobic and H-bonding interactions as it passes from CP-plane to CP-CP interface regions within the nanotube pore.[13d] These distinct environments within the CPN channel impact on the diffusion of water, which requires a driving force to enable diffusion through the antiparallel-stacked environment of a CPN channel, as shown by Zhu *et al*.[17]

In this work, we investigate the factors that control the stability of CP nanotube assemblies to understand how to design stable CP nanostructures. The structure and stability of a range of ionisable CPs are studied by X-ray crystallography, NMR spectroscopy and molecular dynamics simulation. We discuss the considerable complexity of CP assembly by addressing the relative alignment of CPs and the effects of hydrophobic and charged side chain composition.

Results

The factors that contribute to CPN stability are as diverse as they are complex, and not all of them are known or understood. The self-assembly of CPs is influenced by both the conformational preferences of individual CP monomers and interactions between monomers within the supramolecular nanotube assembly. **Figure 2** illustrates potential species that may form in a solution of CP monomers. For a planar CP (**Figure 2a**), the backbone NH and carbonyl groups of all the L-amino acids project in the same direction while the D-amino acids project in the opposite direction, giving rise to two distinct faces (the L-face and the D-face). As a result, there are two possible arrangements of antiparallel dimers that can form depending on whether the H-bonding is through the L-face or the D-face (**Figure 2b**, **2c**). Extended antiparallel nanotubes have alternating L and D H-bond interfaces (**Figure 2d**). The stability of these structures is directly determined by the amino acid composition of the CPs. Additionally, parallel nanotubes comprised of a consistent H-bond interface (**Figure 2e**) are feasible. While parallel H-bonded nanotubes are known to exist, antiparallel H-bonding is often proposed to be the more stable arrangement.[10a, 11a] Finally, CPs can make nonplanar structures stabilised by intramolecular H-bonds, creating folded CPs (**Figure 2f**) and less ordered CP-aggregates (**Figure 2g**).

Peptide design

We designed a series of CPs to investigate the interactions important for CPN stability, particularly regarding side chain interactions and H-bond networks (**Table 1**). The peptides were based on the water-soluble CPs **1** and **2** described previously by our group. CPs **1** and **2** contain equal numbers of aspartic acid and lysine residues and therefore have an overall neutral charge at moderate pH. They have good water solubility and were shown to assemble into fibres by cryo-EM and crystallography. Their general composition of alternating hydrophobic and charged amino acids forms the basis of this structural study. Lower case letters denote D-amino acids, while the symbol "ł" is used to distinguish D-Leu from L-Ile.

Table 1. Cyclic D/L peptides synthesised. Lower case denotes D-amino acids, ł indicates D-Leu, O indicates ornithine.

CP	Sequence	CP	Sequence
1	*cyclo*[(DaKa)$_2$]	**9**	*cyclo*[(EłOł)$_2$]
2	*cyclo*[(DłKł)$_2$]	**10**	*cyclo*(DłDłKłKł)
3	*cyclo*(DłKłDłKf)	**11**	*cyclo*(DłKłKłKł)
4	*cyclo*[(DfKf)$_2$]	**12**	*cyclo*(DłDłDłKł)
5	*cyclo*[(HłKł)$_2$]	**13**	*cyclo*(DłLłKłLł)
6	*cyclo*[(HhLł)$_2$]	**14**	*cyclo*[(KdLł)$_2$]
7	*cyclo*[(EłKł)$_2$]	**15**	*cyclo*[(DłKł)$_3$]
8	*cyclo*[(DłOł)$_2$]		

CPs **3** and **4** are analogues of leucine-containing CP **2** where 1 or 2 D-Leu residues have been replaced with D-Phe. These are more hydrophobic variants of **1** and **2**, with a predicted hydrophobicity ranking of **2** < **3** < **4**.[18] CPs **5** and **6** investigate the incorporation of His residues and are not charge-neutral. CPs **7**-**9** were designed to compare the effects of changing the lengths of the side chains in the charged residues. Ornithine and lysine were used to vary the length of basic side chains and aspartic acid and glutamic acid were used to vary the length of acidic side chains. CPs **10**-**14** vary the numbers and arrangements of Asp, Lys and Leu residues to generate compositionally similar but structurally distinct CPs. CP **15** is a cyclic dodecapaptide that was designed to investigate the assembly of larger CPs. This peptide is similar to CP **2** but contains an additional DłKł segment

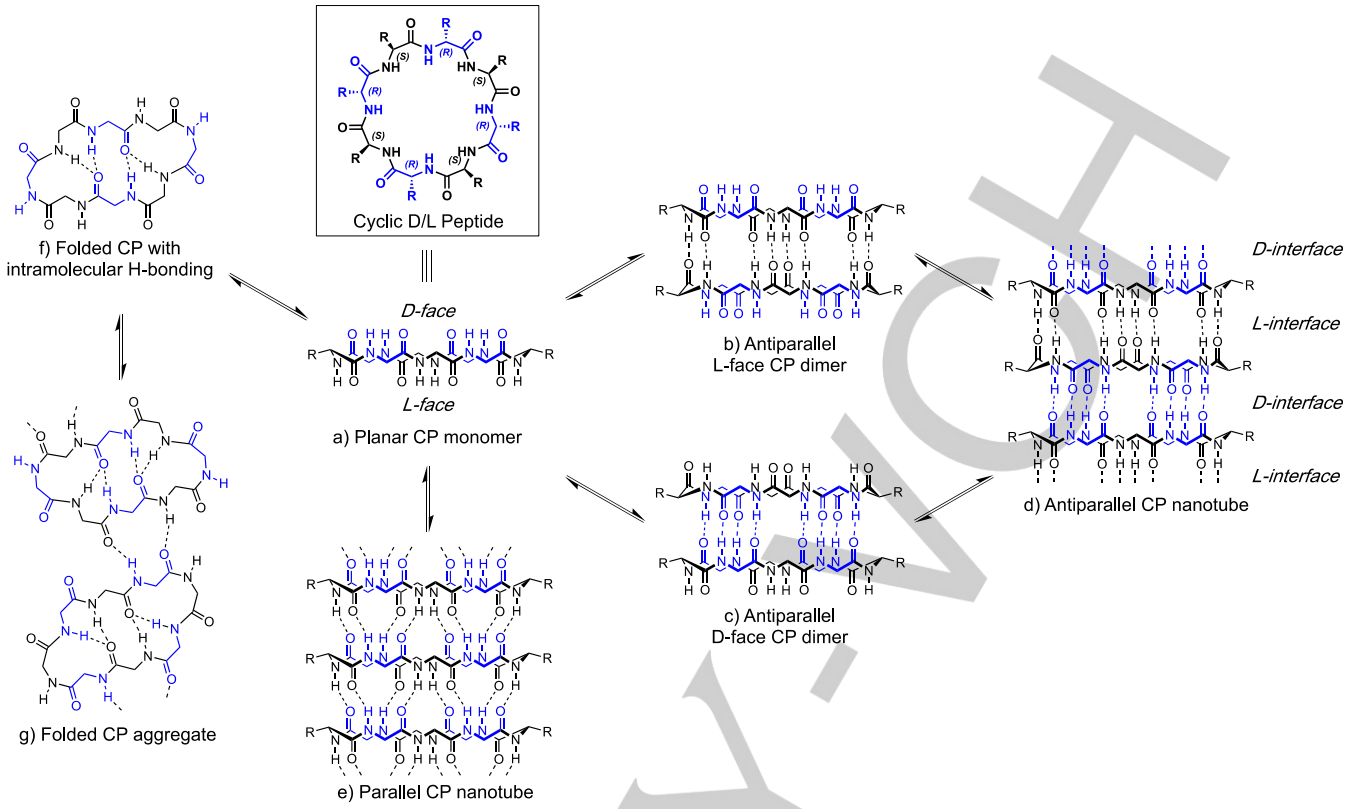

Figure 2. Potential supramolecular structures of cyclic D/L octapeptides. L-amino acids are shown in black and D-amino acids are in blue. a) The planar monomer has two faces (L-face and D-face). b, c) Monomers can assemble through the L- or D- faces to form antiparallel dimers. d) Dimers can further assemble to make antiparallel CP nanotubes. e) Self-assembly can alternatively result in parallel CP nanotubes. f) CP monomers can fold into non-planar conformations stabilised by internal H-bonding. g) Larger (possibly regular) aggregates of nonplanar monomers can form.

Peptide synthesis

All CPs were synthesised using standard Fmoc solid-phase peptide synthesis methods. Linear peptide precursors were synthesised on 2-CTC resin before cleavage with the side chain protecting groups intact. Head-to-tail cyclisation was then performed in solution. Deprotection of the amino acid side chains and purification by preparative HPLC gave the cyclic peptides in moderate to good yields and in high purity.

Peptide crystallisation

We aimed to determine the effects of amino acid composition on the molecular packing of CPs within larger assemblies using X-ray crystallography. Hanging and sitting-drop vapour diffusion experiments were conducted for CPs **1-15** in an effort to generate crystals that were suitable for X-ray diffraction studies. Initial screens used the 'Shotgun' screen[19] before optimization of crystal morphology using additive screens (Hampton Research, USA). Diffraction data for promising crystalline material were collected using the MX2 micro-focus beamline at the Australian Synchrotron.[20]

We have previously crystallised CPs **1** and **2**.[9] CPs **10**, **11** and **12** crystallised as needle-like crystals of up to 100 x 8 x 8 µm, while **8** crystallised as larger needles of up to 1000 x 15 x 15 µm. An additional crystal form of **2** was obtained from novel growth conditions (1.44 M trisodium citrate with 2-5% HFIP) producing diamond-shaped crystals with approximate widths of 100 x 100 x 100 µm. Growth conditions are reported in the supporting information (**Table S1**). CPs **7** and **9** did not produce any crystalline material but instead, consistently generated highly viscous solutions. All remaining CPs formed amorphous non-crystalline aggregates and precipitates.

Minor differences in CP sequence were found to produce marked variations in the crystallisation results. Substitution of Asp with Glu (**2** versus **7** and **8** versus **9**) resulted in the formation of highly viscous solutions rather than crystals. The replacement of Leu residues in CP **2** with Phe (CPs **3** and **4**) or incorporation of many Leu residues (**13**) caused the CPs to produce turbid solutions, likely due to poor solubility and/or CP aggregation. CP **14** also gave highly turbid solutions, despite having the same amino acid composition as the more soluble CPs **2** and **10**.

Solution of crystal structures

Of the CPs that were successfully crystallised, structures could be solved for CPs **2** and **8**. Crystals of **8** diffracted to 1.5 Å with a unit cell of dimensions a = 12.9 Å, b = 17.7 Å, c = 26.4 Å, $\alpha = \beta = \gamma = 90°$ and the structure was solved by dual space methods using SHELXT[21] and refined with SHELXL.[22] Crystals of **2** diffracted to 1.1 Å, but could not be solved by

direct methods. The structure of **2** was ultimately solved by molecular replacement using the crystal-structure backbone of **8** as a search model (unit cell dimensions of a = 17.8 Å, b = 32.6 Å, c = 58.0 Å, $\alpha = \beta = \gamma = 90°$). Molecular replacement was performed in the CCP4 suite[23] using Phaser[24] for initial model fitting, an initial refinement in Refmac[25] and the final refinement in SHELXL.[22]

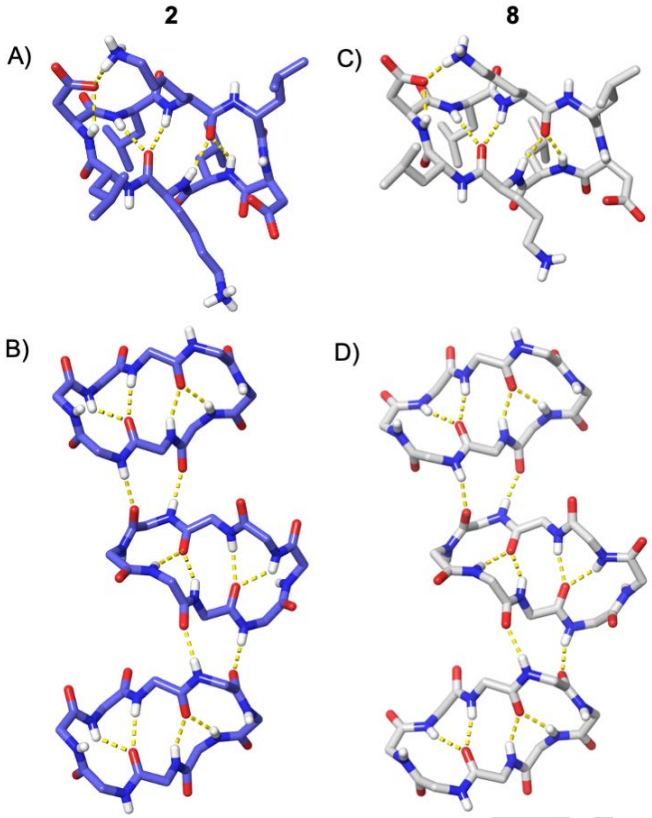

Figure 3. Crystal structures of CPs **2** and **8**. A) CP **2** adopts a folded conformation that is stabilised by three or four intramolecular H-bonds. B) Two intermolecular H-bonds form between each CP subunit for **2**. C & D) CP **8** contains almost identical intra and intermolecular H-bond interactions to **2**.

Both CP **2** (in the new form) and CP **8** were found to crystallise, not as nanotubes, but in an approximately symmetrical, folded conformation that is stabilised by inter- and intramolecular H-bonds. This conformation is similar to that reported for some α,γ-CPs.[8, 16] In this form, the backbone of CP **2** is folded to accommodate three to four intramolecular H-bonds (**Figure 3a**) between the carbonyl of each Lys residue and the backbone NH of the Lys and Leu residues on the opposite side of the CP. Four conformations of **2** exist within the asymmetric unit and 16 CP molecules are contained in the unit cell. All conformations have almost identical backbone conformations with slight variations in the side chain conformations (**Figure S1**). Three of the CP conformations have four intramolecular backbone H-bonds while the fourth conformation has three. In addition to intramolecular H-bonds, there are two intermolecular H-bonds between each CP backbone (**Figure 3b**). The crystal structure of **8** is very similar to **2**. The backbone of CP **8** adopts an almost identical conformation to that of **2** with the same four intramolecular H-bonds being present (**Figure 3c**). For CP **8**, the asymmetric unit contains only one peptide and four in the unit cell, although each CP forms the same two intermolecular H-bonds between adjacent CPs as seen for **2**.

NMR spectroscopy

The stability of CP assemblies in solution was investigated by NMR spectroscopy. The half-lives of the backbone H-bonds were measured using ^{1}H-D exchange at 298 K and pH 3.0. On dissolution in D_2O, the backbone H^N signals exchange with deuterium and decay over time. This decay can be quantified to derive half-life values, providing information about the solvent exposure of the H^N groups and the stability of the H-bonding within the assembly. In addition, the sample turbidity was assessed visually as an indication of CPN assembly and aggregation.

Peptides were dissolved in 100% D_2O at a concentration of 8 mM and 1D ^{1}H NMR spectra were acquired over 60 minutes. For CPs that gave spectra with well-dispersed backbone H^N signals, the H-bond half-lives were calculated for each individual residue in the peptide. For CPs with overlapping H^N signals, half-lives were determined for the amide region as a whole. In all cases, half-lives were averaged to provide an estimate of the overall stability (half-lives were summed and divided by 4 for CPs with two-fold molecular symmetry or divided by 8 for asymmetric CPs).

The exchange experiments show that changes in CP sequence strongly influence CPN stability. The backbone amide protons of the His-containing CPs **5** and **6** were completely unprotected from the solvent and exchanged with deuterium within 10 minutes (CP **5**), or sooner (CP **6**). Ala-rich CP **1**, Asp-rich CP **12** and cyclic dodecapeptide **15** had short half-lives while Asp/Lys-containing CPs **2**, **10** and **14**, Glu/Lys-containing CP **7** and Lys-rich CP **11** had the longest half-lives. CP **14** was poorly soluble at 8 mM and was studied at 4 mM (**Figure S2**). The single substitution of Leu with Phe in CP **3** resulted in an almost 2-fold decrease in H^N half-life when compared with **2**. Lys to Orn substitution in CP **8** reduced H^N half-lives, while the introduction Glu and Orn residues in CP **9** induced substantial turbidity and poor aqueous solubility. CPs **4** and **13** could not be analysed due to poor aqueous solubility caused by hydrophobic Phe residues in CP **4** and high Leu content in **13**. ^{1}H NMR spectra at three timepoints for each CP studied by ^{1}H-D exchange are provided in **Figure S3-13**.

The turbidity of CP solutions gave further insight into the degree of aggregation within different samples. Turbidity was assessed by eye and classified as low, medium or high (**Figure S14**), and was consistent with our measurements of H-bond half-lives. The more turbid samples (CPs **7** and **14**) had longer half-lives while CPs **1**, **5-8** and **15** had short half-lives and low turbidity.

Assembly of CP dimers

CPs can assemble through parallel or antiparallel H-bonding in a β-sheet-like manner. In both parallel and antiparallel systems, the amino acid side chains of each CP align with the

neighbouring monomer. Each amino acid forms two hydrogen bonds (C=O to H-N and N-H to O=C) to the adjacent CP (**Figure 4**). In parallel CP systems, each H-bond is to the residues on either side of the residue with which it is aligned (i.e., residue 5 in CP1 is hydrogen bonded to residues 4 and 6 in CP2). In antiparallel CP systems, the two H-bonds form between the aligned residues (i.e., residue 5 in CP1 makes H-bonds to residue 5 in CP2).

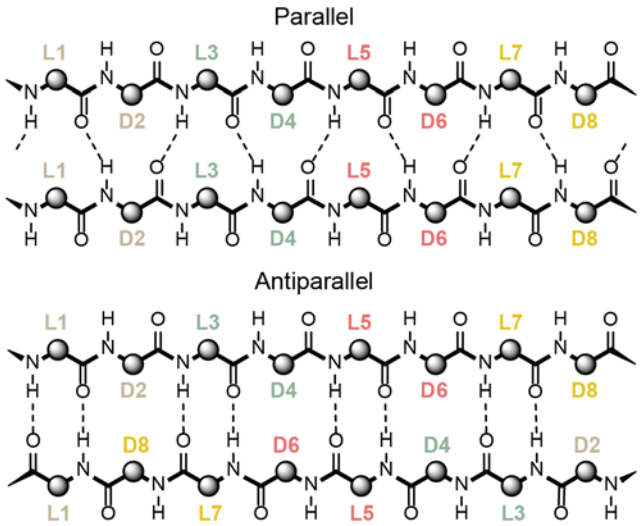

Figure 4. 'Unwrapped' representation of backbone H-bonding in parallel and antiparallel CP dimers. There are two H-bonds per residue. In both cases, amino acid side chains are aligned. In the parallel arrangement, H-bonds are made to the residues on either side of the aligned residue. In the antiparallel arrangement, H-bonds are made directly between the aligned residues.

Examination of the CP dimer structure reveals that multiple distinct H-bonded alignments are possible (**Figure 5**) and that these all need to be considered when analysing CP dimer stability. We will use the term 'alignments' to denote different hydrogen bonded pairings of amino acids. The total number of possible CP dimer alignments depends on 1) the number of residues in the CP, 2) whether the dimer is parallel or antiparallel, 3) whether the dimer is homogeneous or heterogeneous and 4) any symmetry within the individual CP monomers. Here we consider asymmetric octapeptide homodimers. We refer to residues by their sequence number and stereochemistry. For example, an 8-amino acid CP can be represented as *cyclo*(L1-D2-L3-D4-L5-D6-L7-D8). In an 8-amino acid CP, successive 90° rotations of one peptide relative to the other create four different ways to align amino acids. In a parallel dimer, we denote the four alignments as PL1-1, PL1-3, PL1-5 and PL1-7. As an example, alignment 'PL1-3' indicates a parallel dimer aligned with residue L3 of one CP adjacent to L1 of the other. In antiparallel dimers, the interactions can be made through the L-face or the D-face of the CP. Four rotations per face give a total of 8 possible alignments for an antiparallel cyclic D/L octapeptide. These alignments are denoted AL1-1, AL1-3, AL1-5 and AL1-7 for an antiparallel L-face dimer and AD2-2, AD2-4, AD2-6 and AD2-8 for a D-face CP dimer. For symmetrical peptides, where residues 1 to 4 are the same as residues 5 to 8, only two possible alignments exist for each L or D-face where AL1-1, AD2-2, AL1-3 and AD2-4 are equivalent to AL1-5, AD2-6, AL1-7, AD2-8, respectively. **Figure 5** summarises the various distinct alignments of 8-amino acid CPs within an antiparallel dimer.

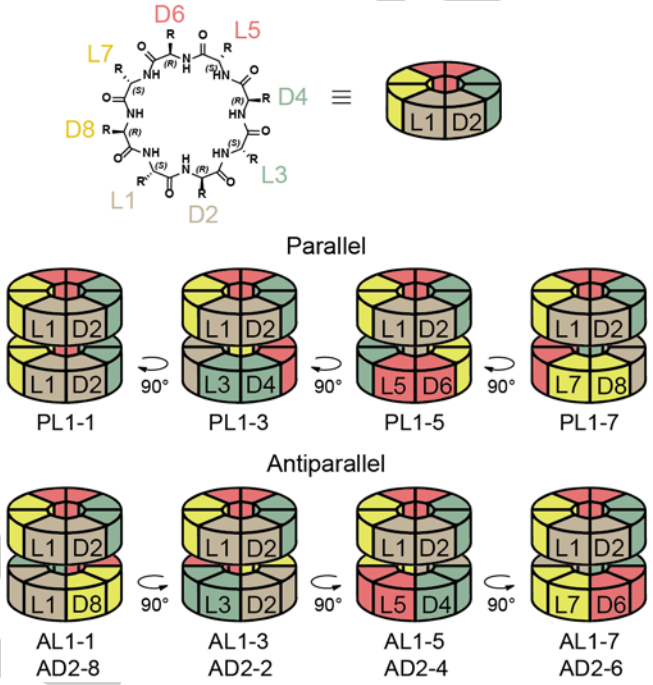

Figure 5. There are four distinct alignments of amino acids within an 8-amino acid CP homodimer. Successive 90° rotations of one monomer generate all possible alignments. Antiparallel dimers can form through the L-face or the D-face giving 8 distinct antiparallel alignments.

Molecular dynamics simulations of CP dimers

MD simulations of CP homodimers in explicit solvent (water) were used to investigate the influence of amino acid side chains on CP-CP stability and to gain additional insight into the experimental measurements of CP assembly. The solvated dimers were modelled using the Desmond MD software (D. E. Shaw Research, version 4.3). Systems were built in 35 × 35 × 35 Å orthorhombic cells with periodic boundary conditions and solvated with explicit water containing 0.15 M NaCl to more closely model a biological system (**Figure 6a**). Ionisable side chains (His, Orn, Lys, Asp and Glu) were considered to be charged. Simulations were run at 300 K and 1.01 bar for 100 ns. Multiple individual simulations were run for each CP dimer, testing all possible parallel and antiparallel alignments. The average number of intermolecular backbone-backbone H-bonds was calculated for each simulation and used as a measure of dimer stability. In stable CP dimers, the CPs remained associated throughout the 100 ns simulation, while the CPs of an unstable dimer fell apart.

Figure 6 illustrates a set of simulations performed on the antiparallel CP **2** dimer. The dimer was modelled in its four possible H-bonded alignments (**Figure 6b**). The AD2-2 alignment was found to be the most stable (**Figure 6c**), with no dissociation of the dimer for the full duration of the simulation

(**Figure 6d, 6e**). The most stable alignments of CP **2** arose from Leu-Leu H-bonding in the D-interface of CP dimers (alignments AD2-2, AD2-4), while the AL1-1 and AL1-3 alignments caused the dimer to fall apart.

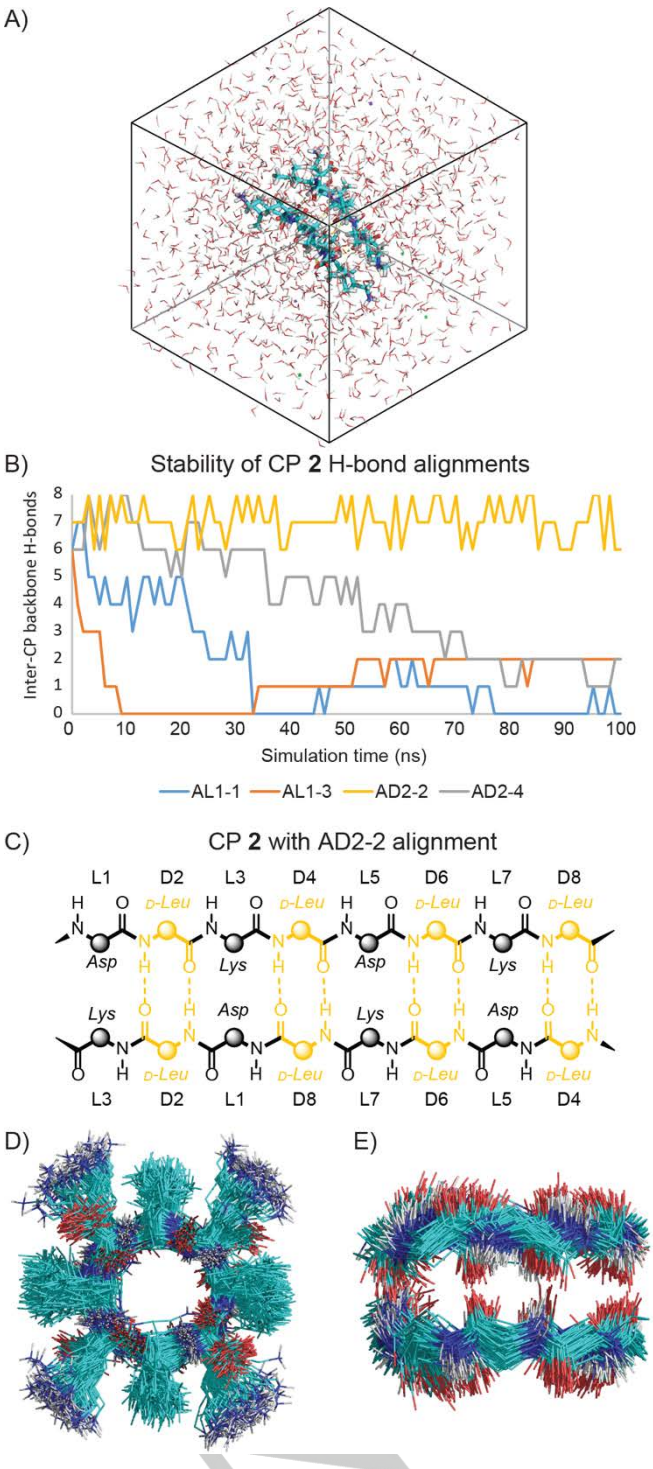

Figure 6. A) MD simulation system of a CP **2** dimer in explicit water containing 0.15M NaCl. B) The number of intermolecular backbone H-bonds (Y-axis) present over the course of 100 ns MD simulations of each of the four possible antiparallel alignments of the CP **2** dimer. C) AD2-2 was the most stable dimer alignment for CP **2** and composed entirely of Leu-Leu H-bonds. D) Overlay of all frames from the AD2-2 simulation of CP **2** showing the structural stability of this arrangement. E) Side-view of CP **2** (AD2-2) showing the peptide backbone only.

All parallel CP dimers investigated were found to be unstable (**Table S3**) with dissociation occurring within 1 ns. In contrast, the antiparallel dimers varied between being stable during the 100 ns simulation and rapidly dissociating. Dimer stability was dependent on the particular alignment of amino acids and no CP dimer was stable in all of its possible antiparallel alignments. The average number of backbone intermolecular H-bonds over the course of a 100 ns MD simulation for each CP in each antiparallel alignment is presented in **Table 2**. Most of the CPs were found to have at least one antiparallel alignment that remained stable for the full 100 ns. CPs **1, 6** and **12** were found to be very unstable, with all alignments resulting in the disassembly of the CP dimers. CPs **7**, **11** and **14** had stable alignments in both the L and D interfaces, indicating that these CPs may form highly stable nanotube assemblies.

A number of interesting observations can be made from our simulations of this set of CP analogues, particularly regarding side chain hydrophobicity, opposing or matching charge-charge interactions and the backbone H-bonding interfaces.

Side chain hydrophobicity had a strong impact on CP dimer stability. More hydrophobic CPs, containing Phe (CPs **3** and **4**) or many leucine residues (CP **13**), were generally more stable. CP **3** was stable in all D-interface alignments with a single D-Phe, while **4** with four D-Phe residues was more stable in the L-interface in addition to being stable in all D-interface alignments. However, **13** was only stable in two D-interface alignments despite high Leu-content, suggesting that increasing side chain hydrophobicity does not necessarily improve H-bond stability.

CP dimers with oppositely-charged side chains aligned were stable in many cases, but were highly dependent on the side chain lengths. Asp, Orn and His have short side chains while Glu and Lys have longer side chains. The most stable alignments of opposing charge were Glu-Orn, Glu-Lys and Asp-Orn (CPs **7**-**9**, alignments AL1-3 / AL1-7). Asp-Lys alignment was only stable in D-interface dimers (alignments AD2-2, AD2-6 of CPs **2**-**4** and **15**). CP dimers of **7**-**9** were more stable than **2,** possibly due to the closer matching of side chain length in **7**-**9** facilitating ionic interactions. The shorter, polar Asp side chain terminal lies near the non-polar mid-section of the longer Lys side chain and may contribute to the instability of dimers with such an alignment.

Simulations where negatively charged side chains were aligned were unstable with the exception of CP **14** in the AD2-2 / AD2-6 alignment. In this case, the favourable hydrophobic Leu-Leu interactions counteracted the repulsive Asp-Asp interactions. The alignment of positively-charged Lys residues was not as detrimental to stability, possibly due to greater length and flexibility of the Lys side chains, which allows greater distance between like-charges without forcing dimer dissociation. The contrast between the negatively and positively charged side chains is reflected by CP **11** (3 Lys and 1 Asp) and **12** (3 Asp and 1 Lys**).** CP **11** had 4 stable alignments while Asp-rich **12** had none. Charge-matching of His residues had interesting effects on CP dimer stability. It produced a stable alignment in CP **5** when His residues were aligned and H-bonded to each other (AL1-1 / AL1-3) but was

very unstable when His residues were aligned but not H-bonded to each other (AD2-4, AD2-8). High numbers of His residues in CP **6** resulted in complete instability in all alignments, all of which suggests that CPs containing His are particularly sensitive to inter and intramolecular side chain distances and alignments.

Table 2. The average number of intermolecular backbone H-bonds for CP dimers in antiparallel alignments from MD simulations.

		Dimer alignments								Total of stable simulations		
CP	Sequence	AL1-1	AL1-3	AL1-5	AL1-7	AD2-8	AD2-2	AD2-4	AD2-6	L	D	All
1[a]	*cyclo*[(DaKa)$_2$]	3.1	1.4	3.1	1.4	2.8	3.7	2.8	3.7	-	-	0
2[a]	*cyclo*[(DłKł)$_2$]	3.3	1.8	3.3	1.8	5.8	7.0	5.8	7.0	-	2	2
3	*cyclo*(DłKłDłKf)	3.5	1.1	4.6	1.0	6.9	7.1	7.0	7.0	-	4	4
4[a]	*cyclo*[(DfKf)$_2$]	4.5	1.3	4.5	1.3	7.4	7.6	7.4	7.6	-	4	4
5[a]	*cyclo*[(HłKł)$_2$]	7.3	4.3	7.3	4.3	0.4	5.0	0.4	5.0	2	-	2
6[a]	*cyclo*[(HhLł)$_2$]	0.2	1.5	0.2	1.5	2.2	1.4	2.2	1.4	-	-	0
7[a]	*cyclo*[(ElKł)$_2$]	4.1	7.4	4.1	7.4	6.7	2.7	6.7	2.7	2	2	4
8[a]	*cyclo*[(DłOł)$_2$]	2.8	7.6	2.8	7.6	5.4	1.2	5.4	1.2	2	-	2
9[a]	*cyclo*[(ElOł)$_2$]	3.0	7.2	3.0	7.2	4.2	5.5	4.2	5.5	2	-	2
10	*cyclo*(DłDłKłKł)	1.9	1.5	2.1	0.8	3.7	6.7	6.6	6.2	-	2	2
11	*cyclo*(DłKłKłKł)	2.2	3.4	6.9	6.0	7.0	7.1	3.5	4.6	2	2	4
12	*cyclo*(DłDłDłKł)	0.2	0.8	0.4	0.3	1.4	6.0	5.9	6.1	-	-	0
13	*cyclo*(DłLłKłLł)	3.6	3.5	2.2	6.1	7.3	5.0	7.2	2.0	-	2	2
14[a]	*cyclo*[(KdLł)$_2$]	4.1	7.0	4.1	7.0	0.7	5.9	0.7	5.9	2	2	4
15[a,b]	*cyclo*[(DłKł)$_3$]	0.7	1.9	0.7	1.9	4.8	7.0	4.8	7.0	-	2	2

[a] In these peptides, the alignments AL1-1, AD2-2, AL1-3, AD2-4 are equivalent to AL1-5, AD2-6, AL1-7 and AD2-8 respectively, due to symmetry. [b] To compare with 8-amino acid CPs, the number of H-bonds is adjusted by a factor of 2/3. CP **15** has 3-fold symmetry and has 4 unique dimer alignments.

CP dimers formed through the L-interface and D-interfaces had significantly different stabilities (**Table 2**). In many cases, dimers were stable through one interface (L or D). For example, dimers of CPs **7-9** were completely stable when opposing charge side chains were aligned with backbone H-bonding through the L-interface (alignments AL1-3 / AL1-7) but unstable with the same side chain alignments but with H-bonding through the D-interface (alignments AD2-2 / AD2-6).

Comparison of the experimental and computational data shows that the MD studies have predictive power. **Table 3** shows the NMR spectroscopy, turbidity and MD data sorted according to the NMR spectroscopy-derived half-lives. CP dimers with stable H-bond alignments by MD simulation had longer H-bond half-lives as determined experimentally by NMR spectroscopy. Likewise, dimers with no stable alignments by MD had shorter H-bond half-lives by NMR spectroscopy. Furthermore, a CP dimer with stable alignments in both D and L interfaces by MD study would potentially form an extended nanotube with stable H-bond interfaces throughout the entire structure. This was evident for CPs **7**, **11** and **14**, which had stable arrangements in both the D and L interfaces by MD and long exprerimental half-lives with high turbidity. We note that the MD simulations run here are limited to CP dimers that are just one of the potential species that could form in solution (**Figure 2**). However, theoretical studies of dimers are simpler than extended nanostructures, which allows for in-depth analysis of the features critical to CP-CP stability.

Table 3. CP assembly stability by different measures, ordered by average $t_{1/2}$.

CP	Sequence	$t_{1/2}$ avg (min)	Turbidity	Stable MD[a]
4	*cyclo*[(DfKf)$_2$]	- [b]	High	4/8
9	*cyclo*[(EłOł)$_2$]	- [b]	High	2/8
13	*cyclo*(DłLłKłLł)	- [b]	High	2/8
2	*cyclo*[(DłKł)$_2$]	12.5	Med	2/8
14	*cyclo*[(KdLł)$_2$]	12.0[c]	High	4/8
10	*cyclo*(DłDłKłKł)	11.4	Med	2/8
11	*cyclo*(DłKłKłKł)	10.1	Med	4/8
7	*cyclo*[(EłKł)$_2$]	10.0	High	4/8
8	*cyclo*[(DłOł)$_2$]	8.7	Low	2/8
3	*cyclo*(DłKłDłKf)	6.0	Med	4/8
12	*cyclo*(DłDłDłKł)	4.4	Med	0/8
15	*cyclo*[(DłKł)$_3$]	4.1	Low	3/12
1	*cyclo*[(DaKa)$_2$]	3.2	Low	0/8
5	*cyclo*[(HłKł)$_2$]	0.5	Low	2/8
6	*cyclo*[(HhLł)$_2$]	~0.0	Low	0/8

[a] Number of dimer alignments stable after 100 ns. [b] Not measured due to very poor solubility. [c] Measured at 4 mM due to poor solubility.

Discussion

Examination of possible dimer structures shows that many possible arrangements exist for each CP dimer (**Figure 5**) and we describe a simple notation for the different possible associations of CP dimers. Our MD simulations show that different alignments of monomers within CP dimers greatly influences dimer stability; all parallel dimers were found to be unstable in water and antiparallel dimer arrangements varied between being unstable and completely stable in a 100 ns MD simulation.

This study shows that inter-side chain hydrophobic interactions are particularly beneficial for dimer stability. For example, CP **4** contains four Phe residues and was stable in all D-interface dimer alignments in the MD simulations. A disadvantage, however, of increasing the side chain hydrophobicity is poor aqueous solubility, as seen for CP **4**. CP **1**, which contains less hydrophobic alanine in the place of Phe, has significantly improved aqueous solubility but much lower H-bond stability as measured by both MD simulations and NMR spectroscopy.

We also find that inter-CP charge interactions strongly influence the stability of CPN assemblies. The MD studies show that the alignment of opposite charges stabilises antiparallel CP dimers while alignment of like-charges often caused complete dimer dissociation. Although the previously reported crystal structures[9] of **1** and **2** have aligned like-charges, this arrangement is stabilised in the crystal lattice by opposing charge groups of adjacent nanotubes.

The crystallography studies performed here and previously[9] also highlight the role of side chain interactions in CPN stability. CPs with similar amino acid compositions have crystallised with varied crystal morphologies. We have found folded CP aggregates (CPs **2** and **8**), parallel H-bonded nanotubes (**1**) and antiparallel H-bonded nanotubes (**2**).

There is good correlation between the theoretical MD studies and experimental NMR spectroscopic analysis. CP dimers with stable H-bond alignments by MD had longer H-bond half-lives by NMR spectroscopy, while unstable CPs by MD had much shorter half-lives. Although we only applied our MD studies to CP dimers, the good correlation between the MD and experimental findings indicates that this information could be applied to extended nanostructures.

Conclusions

In this work we investigated the influence of sidechain-sidechain interactions on nanotube assembly (**Figure 1**) through crystallography, NMR spectroscopy and computational methods. Crystallography studies of the peptides produced folded conformations for two of the CPs. These folded conformations are alternate, non-nanotube conformations that can be expected to compete with nanotube formation in solution. Examination of the CP dimer structure shows that a homogeneous CP dimer can be assembled in many different alignments. This work shows that CP dimer stability is highly dependent on the amino acid sequence and the dimer alignment. MD simulations of parallel dimers were unstable in all arrangements and significant differences were seen in the stabilities of the L and D-interfaces in many antiparallel CP dimers.

Molecular dynamics and NMR spectroscopy studies showed that the incorporation of hydrophobic amino acids improved dimer stability through inter-CP side chain interactions, although increasing the number of hydrophobic amino acids also reduced aqueous solubility. Alignment of side chains with opposite charges improved overall dimer stability provided that the side chains were of similar length, while the alignment of negative charges destabilised the nanotubes. Nanostructures that are stable in water will most likely require a mix of charged and hydrophobic residues.

This work extends our understanding of the factors contributing to the stability of CPNs by exploring inter-CP charge interactions, hydrophobic interactions and relative CP alignment. Although we simplified modelling complex CPN structures by considering only CP dimers, we found a useful correlation between the stability measured by MD results and NMR spectroscopy measurements of H-bond lifetime. Our findings in the importance of charged sidechain length on CPN stability are consistent with studies of β-sheet structures.[26] CPN stability depends on the relative alignment of CPs, as found by Liu et al in similar systems,[13d] in addition to the distinct H-bond interfaces that can form.

Overall, the work described here will assist us to engineer the stability of inter-CP H-bond interfaces and direct the pattern of assembly by careful control of amino acid composition. In the future, we will apply these findings to design more extended nanostructures.

Experimental Section

Cyclic peptide synthesis: *Coupling of the first amino acid:* 2-chlorotrityl chloride resin (83 mg, resin loading 1.2 mmol g^{-1}, 0.1 mmol) was swelled in 5 mL of CH_2Cl_2 for 30 min in a sinter-fitted syringe. The resin was then drained and treated with 1 equivalent (relative to resin capacity) of Fmoc-amino acid dissolved in CH_2Cl_2 (4 mL). To the resin mixture was added 6 equivalents of DIPEA relative to amino acid and the resulting mixture was agitated at room temperature overnight. The resin was drained and washed with DMF (3 x 3 mL) and treated with MeOH (2 x 3 mL) to cap any unreacted sites. The resin was then washed with DMF (3 x 3 mL) and transferred to an SPPS reaction vessel. *Automated synthesis of linear peptides:* The linear peptides were prepared using an automated solid-phase peptide-synthesiser (Protein Technologies Inc. PS3). On each coupling cycle, the resin was first washed with DMF (3 x 30 s). Fmoc deprotection was achieved using 20% piperidine in DMF (2 x 5 min) followed by washing with DMF (6 x 30 s) to provide the resin-bound free amino-terminal of the peptide. Amino acid couplings used three equivalents of Fmoc amino acid and 2-(6-chloro-1H-benzotriazole-1-yl)-1,1,3,3-tetramethylaminium hexafluorophosphate (HCTU), relative to resin loading. The amino acid and HCTU were dissolved in a solution of 7% DIPEA in DMF. The solution was added to the resin which was agitated at room temperature for 1 h, drained and washed with DMF (3 x 30 s). After coupling the final amino acid, a further Fmoc deprotection was performed to obtain the resin-bound peptide with free amino terminal. The resin was transferred to a sinter-fitted syringe and washed with DMF (3 x 3 mL), MeOH (3 x 3 mL) and Et_2O (3 x 3 mL). *Peptide cleavage from resin:* The resin-bound linear peptide was treated with a solution of 20% 1,1,1,3,3,3-hexafluoroisopropanol (HFIP) in CH_2Cl_2 (3 x 3 mL x 10 min) and the HFIP washings were collected by filtration. The resin was then washed with CH_2Cl_2 (3 x 3 mL). The combined HFIP and CH_2Cl_2 washings were concentrated under reduced pressure and freeze-dried from 1:1 ACN/H_2O to yield the side chain-protected linear peptide as a white powder. A sample of the peptide was deprotected and analysed by LCMS to confirm the linear sequence. *Cyclisation:* The linear peptide was added to DMF (7 mg/mL) and treated with 3 equivalents of PyClock and 6 equivalents of DIPEA. The solution was stirred at room temperature for 2 days before being concentrated under reduced pressure to yield a thick oil. The oil was freeze-dried from 1:1 ACN/H_2O to yield the crude side chain-protected cyclic peptide as an off-white solid. *Deprotection:* The side chain protecting groups of the cyclic peptide were removed by treatment with a solution of TFA/TIPS/H_2O (95:2.5:2.5 v/v, 2 mL) for 3 h. The TFA was evaporated using a stream of N_2 gas and the remaining oil was then treated with ice-cold Et_2O to precipitate the peptide. The precipitate was collected by centrifugation and freeze-dried from 1:1 ACN/H_2O to yield the crude cyclic deprotected peptide as a white solid. *Purification:* Peptides were purified by preparative reverse-phase HPLC using a Waters Associates liquid chromatography system (Model 600 Controller and Waters 486 Tunable Absorbance Detector) with a Phenomenex Luna C8(2) 100 Å, 10 µm, 250 x 21.2 mm column with 0.1% TFA/H_2O as buffer A and 0.1% TFA/ACN as buffer B with a flow rate of 10 mL/min.

Analysis: Linear peptides and final CP products were analysed by liquid chromatography mass spectrometry conducted with a Phenomenex Luna C8(2) 100 Å, 3 µm, 100 x 2.0 mm reverse-phase column. Running buffer consisted of solvent A with 0.05% TFA/H_2O and solvent B with 0.05% TFA/ACN. Final CP products were analysed by high-resolution mass spectrometry in 50% ACN/water, and by NMR spectroscopy at 2 mM in DMSO-*d6* at 400 MHz using a 400 MHz Bruker Avance III Nanobay spectrometer.

CPs 1, 2, 5: Synthesis and characterisation previously reported.[9]

CP3: *Linear:* H-Asp(tBu)-D-Leu-Lys(Boc)-D-Phe-Asp(tBu)-D-Leu-Lys(Boc)-D-Leu-OH. White powder, 53.7% yield, MS-ESI (deprotected): $[M + H]^+$ 991.95, $[M + 2H]^{2+}$ 496.80. *Cyclic: cyclo*(Asp-D-Leu-Lys-D-Leu-Asp-D-Leu-Lys-D-Phe). Purification gradient: 20-60% buffer B over 60 min, R_T = 25.5 min (37.0% B). Yield: 14.7 mg (27.5%) as a white solid. ^{1}H NMR (400 MHz, DMSO-*d6*) δ 12.28 (s, 2H), 8.37 – 8.16 (m, 5H), 8.11 (d, *J* = 7.1 Hz, 1H), 8.04 – 7.94 (m, 2H), 7.63 (s, 6H), 7.29 – 7.15 (m, 5H), 4.66 – 4.53 (m, 3H), 4.46 – 4.27 (m, 5H), 2.92 (m, 2H), 2.79 – 2.60 (m, 7H), 2.39 – 2.27 (m, 2H), 1.65 – 1.32 (m, 16H), 1.28 – 1.08 (m, 5H), 0.96 – 0.73 (m, 17H). HRMS (ESI) $[M + Na]^+$ calculated: 995.5536, found: 995.5537, $[M + H]^+$ calculated: 973.5717, found: 973.5727, $[M + 2H]^{2+}$ calculated: 487.2895, found: 487.2913.

CP4: *Linear:* H-Asp(tBu)-D-Phe-Lys(Boc)-D-Phe-Asp(tBu)-D-Phe-Lys(Boc)-D-Phe-OH. White powder, 58.5% yield, MS-ESI (deprotected): $[M + H]^+$ 1094.00, $[M + 2H]^{2+}$ 547.80. *Cyclic: cyclo*[(Asp-D-Phe-Lys-D-Phe)$_2$]. Purification gradient: 0-50% buffer B over 60 min, R_T = 50.4 min (41.9% B). Yield: 9.9 mg (18.1%) as a white solid. ^{1}H NMR (400 MHz, DMSO-*d6*) δ 12.13 (s, 2H), 8.29 (d, *J* = 8.3 Hz, 2H), 8.21 (t, *J* = 9.1 Hz, 4H), 7.98 (d, *J* = 8.4 Hz, 2H), 7.53 (s, 6H), 7.20 – 7.04 (m, 20H), 4.67 – 4.52 (m, 6H), 4.25 (dd, *J* = 13.9, 7.6 Hz, 2H), 2.88 – 2.72 (m, 5H), 2.68 – 2.59 (m, 3H), 2.57 – 2.48 (m, 6H), 2.17 – 2.00 (m, 5H), 1.25 – 1.13 (m, 6H), 0.98 (m, 4H), 0.81 – 0.57 (m, 5H). HRMS (ESI) $[M + Na]^+$ calculated: 1097.5067, found: 1097.5048, $[M + H]^+$ calculated: 1075.5247, found: 1075.5258, $[M + 2H]^{2+}$ calculated: 538.2660, found: 538.2679.

CP6: *Linear:* H-His(Trt)-D-His(Trt)-Leu-D-Leu-His(Trt)-D-His(Trt)-Leu-D-Leu-OH. White powder, 70.4% yield, MS-ESI (deprotected): $[M + H]^+$ 1019.85, $[M + 2H]^{2+}$ 510.70. *Cyclic: cyclo*[(His-D-His-Leu-D-Leu)$_2$]. Purification gradient: 0-60% buffer B (0.1% TFA in 90% ACN/H_2O) over 60 min, R_T = 33.5 min (30.1% ACN/H_2O). Yield: 13.1 mg (37.4%) as a white solid from half of the linear precursor. ^{1}H NMR (400 MHz, DMSO-*d6*) δ 8.96 (s, 1H), 8.94 (s, 1H), 8.50 (d, *J* = 9.3 Hz, 1H), 8.37 (t, *J* = 8.4 Hz, 2H), 8.25 (d, *J* = 8.8 Hz, 1H), 7.33 (s, 1H), 7.24 (s, 1H), 4.86 – 4.74 (m, 2H), 4.49 (td, *J* = 9.2, 4.9 Hz, 1H), 4.41 – 4.33 (m, 1H), 3.04 – 2.82 (m, 4H), 2.74 (dd, *J* = 15.1, 9.2 Hz, 2H), 1.39 – 1.02 (m, 6H), 0.88 – 0.65 (m, 12H). HRMS (ESI) $[M + H]^+$ calculated: 1001.5792, found: 1001.5796, $[M + 2H]^{2+}$ calculated: 501.2932, found: 501.2948, $[M + 3H]^{3+}$ calculated: 334.5312, found: 334.5330.

CP7: *Linear:* H-Glu(tBu)-D-Leu-Lys(Boc)-D-Leu-Glu(tBu)-D-Leu-Lys(Boc)-D-Leu-OH. White powder, 50.4% yield, MS-ESI (deprotected): $[M + H]^+$ 986.05, $[M + 2H]^{2+}$ 493.85. *Cyclic: cyclo*[(Glu-D-Leu-Lys-D-Leu)$_2$]. Purification gradient: 20-60% buffer B over 60 min, R_T = 21.1 min (34.1% B). Yield: 7.4 mg (15.3%) as a white solid. ^{1}H NMR (400 MHz, DMSO-*d6*) δ 12.03 (s, 1H), 8.23 – 8.00 (m, 4H), 7.54 (s, 3H), 4.46 – 4.25 (m, 4H), 2.66 (dt, *J* = 12.7, 6.3 Hz, 2H), 2.10 (dt, *J* = 10.0, 7.2 Hz, 2H), 1.86 – 1.72 (m, 2H), 1.72 – 1.09 (m, 18H), 0.86 – 0.71 (m, 12H). HRMS (ESI) $[M + Na]^+$ calculated: 989.6006, found: 989.5985, $[M + H]^+$ calculated: 967.6186, found: 967.6192, $[M + 2H]^{2+}$ calculated: 484.313, found: 484.3146.

CP8: *Linear:* H-Asp(tBu)-D-Leu-Orn(Boc)-D-Leu-Asp(tBu)-D-Leu-Orn(Boc)-D-Leu-OH. White powder, 59.6% yield, MS-ESI (deprotected): $[M + H]^+$ 929.95, $[M + 2H]^{2+}$ 465.75. *Cyclic: cyclo*[(Asp-D-Leu-Orn-D-Leu)$_2$]. Purification gradient: 20-60% buffer B over 60 min, R_T = 25.5 min (37.0% B). Yield: 11.3 mg (31.3%) as a white solid. ^{1}H NMR (400 MHz, DMSO-*d6*) δ 12.35 (s, 1H), 8.29 (d, *J* = 6.9 Hz, 2H), 8.02 (dd, *J* = 27.5, 6.8 Hz, 2H), 7.66 (s, 3H), 4.60 (dd, *J* = 12.6, 6.5 Hz, 1H), 4.50 – 4.27 (m, 3H), 2.76 (d, *J* = 19.5 Hz, 2H), 2.63 (ddd, *J* = 24.6, 10.1, 5.5 Hz, 2H), 1.73 – 1.23 (m, 11H), 0.94 – 0.70 (m, 12H). HRMS (ESI) $[M + Na]^+$ calculated: 933.5380, found: 933.5366, $[M + H]^+$ calculated: 911.5560, found: 911.5568, $[M + 2H]^{2+}$ calculated: 455.2738, found: 455.2780.

CP9: *Linear:* H-Glu(tBu)-D-Leu-Orn(Boc)-D-Leu-Glu(tBu)-D-Leu-Orn(Boc)-D-Leu-OH. White powder, 47.9% yield, MS-ESI (deprotected): $[M + H]^+$ 958.00, $[M + 2H]^{2+}$ 479.80. *Cyclic: cyclo*[(Glu-D-Leu-Orn-D-Leu)$_2$].

Purification gradient: 20-60% buffer B over 60 min, R_T = 21.0 min (34.0% B). Yield: 10.5 mg (22.6%) as a white solid. ^{1}H NMR (400 MHz, DMSO-*d*$_6$) δ 12.10 (s, 1H), 8.28 – 8.19 (m, 3H), 8.16 (d, *J* = 8.8 Hz, 1H), 7.65 (s, 3H), 4.56 – 4.40 (m, 4H), 2.84 – 2.73 (m, 2H), 2.16 (dd, *J* = 15.3, 9.4 Hz, 2H), 1.91 – 1.20 (m, 14H), 0.97 – 0.77 (m, 12H). HRMS (ESI) $[M + Na]^+$ calculated: 961.5693, found: 961.5689, $[M + H]^+$ calculated: 939.5873, found: 939.5883, $[M + 2H]^{2+}$ calculated: 470.2973, found: 470.2988.

CP10: *Linear:* H-Lys(Boc)-D-Leu-Asp(tBu)-D-Leu-Asp(tBu)-D-Leu-Lys(Boc)-D-Leu-OH. White powder, 61.4% yield, MS-ESI (deprotected): $[M + H]^+$ 958.00, $[M + 2H]^{2+}$ 479.85. *Cyclic: cyclo*(Asp-D-Leu-Asp-D-Leu-Lys-D-Leu-Lys-D-Leu). Purification gradient: 20-60% buffer B over 60 min, R_T = 24.8 min (36.5% B). Yield: 14.2 mg (41.4%) as a white solid. ^{1}H NMR (400 MHz, DMSO-*d*$_6$) δ 12.37 (s, 2H), 8.28 – 8.06 (m, 6H), 7.98 (d, *J* = 7.9 Hz, 1H), 7.86 (d, *J* = 8.7 Hz, 1H), 7.64 (s, 6H), 4.61 (qd, *J* = 7.9, 2.4 Hz, 2H), 4.41 – 4.20 (m, 6H), 2.80 – 2.55 (m, 8H), 1.71 – 1.17 (m, 26H), 0.93 – 0.75 (m, 24H). HRMS (ESI) $[M + Na]^+$ calculated: 961.5693, found: 961.5681, $[M + H]^+$ calculated: 939.5873, found: 939.5884, $[M + 2H]^{2+}$ calculated: 470.2973, found: 470.2990.

CP11: *Linear:* H-Asp(tBu)-D-Leu-Lys(Boc)-D-Leu-Lys(Boc)-D-Leu-Lys(Boc)-D-Leu-OH. White powder, 54.2% yield, MS-ESI (deprotected): $[M + H]^+$ 971.05, $[M + 2H]^{2+}$ 486.25. *Cyclic: cyclo*(Asp-D-Leu-Lys-D-Leu-Lys-D-Leu-Lys-D-Leu). Purification gradient: 20-60% buffer B over 60 min, R_T = 24.0 min (36.0% B). Yield: 12.4mg (36.1%) as a white solid on 0.1 mmol scale synthesis. ^{1}H NMR (400 MHz, DMSO-*d*$_6$) δ 12.36 (s, 1H), 8.28 (d, *J* = 7.9 Hz, 1H), 8.20 (dd, *J* = 10.9, 9.0 Hz, 2H), 8.16 – 7.95 (m, 5H), 7.68 (s, 8H), 4.63 (dd, *J* = 13.7, 7.8 Hz, 1H), 4.46 – 4.32 (m, 7H), 2.82 – 2.54 (m, 10H), 1.69 – 1.19 (m, 36H), 0.94 – 0.77 (m, 24H). HRMS (ESI) $[M + H]^+$ calculated: 952.6554, found: 952.6561, $[M + 2H]^{2+}$ calculated: 476.8313, found: 476.8327, $[M + 3H]^{3+}$ calculated: 318.2233, found: 318.2245.

CP12: *Linear:* H-Asp(tBu)-D-Leu-Asp(tBu)-D-Leu-Asp(tBu)-D-Leu-Lys(Boc)-D-Leu-OH. White powder, 53.1% yield, MS-ESI (deprotected): $[M + H]^+$ 944.90, $[M + 2H]^{2+}$ 473.25. *Cyclic: cyclo*(Asp-D-Leu-Asp-D-Leu-Asp-D-Leu-Lys-D-Leu). Purification gradient: 20-60% buffer B over 60 min, R_T = 34.9 min (43.3% B). Yield: 10.6 mg (20.8%) as a white solid. ^{1}H NMR (400 MHz, DMSO-*d*$_6$) δ 12.35 (s, 3H), 8.31 – 8.17 (m, 3H), 8.08 (d, *J* = 6.9 Hz, 1H), 8.04 – 7.93 (m, 3H), 7.70 (d, *J* = 8.2 Hz, 1H), 7.62 (s, 3H), 4.66 – 4.52 (m, 3H), 4.44 – 4.35 (m, 1H), 4.31 – 4.20 (m, 3H), 4.19 – 4.11 (m, 1H), 2.80 – 2.54 (m, 9H), 1.71 – 1.20 (m, 20H), 0.95 – 0.72 (m, 24H). HRMS (ESI) $[M + Na]^+$ calculated: 948.5013, found: 948.5019, $[M + H]^+$ calculated: 926.5193, found: 926.5206, $[M + 2H]^{2+}$ calculated: 463.7633, found: 463.7650.

CP13: *Linear:* H-Lys(Boc)-D-Leu-Leu-D-Leu-Asp(tBu)-D-Leu-Leu-D-Leu-OH. White powder, 65.7% yield, MS-ESI (deprotected): $[M + H]^+$ 941.05, $[M + 2H]^{2+}$ 471.35. *Cyclic: cyclo*(Asp-D-Leu-Leu-D-Leu-Lys-D-Leu-Leu-D-Leu). Yield: 63.0 mg of crude peptide at 41.8% purity as a white solid. MS-ESI: $[M + H]^+$ 923.05, $[M + 2H]^{2+}$ 462.35.

CP14: *Linear:* H-D-Leu-Lys(Boc)-D-Asp(tBu)-Leu-D-Leu-Lys(Boc)-D-Asp(tBu)-Leu-OH. White powder, 69.3% yield, MS-ESI (deprotected): $[M + H]^+$ 957.75, $[M + 2H]^{2+}$ 479.60. *Cyclic: cyclo*[(Lys-D-Asp-Leu-D-Leu)$_2$]. Purification gradient: 0-60% buffer B over 60 min, R_T = 28.2 min (28.2% B). Yield: 6.5 mg (10.0%) as a white solid. ^{1}H NMR (400 MHz, DMSO-*d*$_6$) δ 8.31 (d, *J* = 6.5 Hz, 1H), 8.27 (d, *J* = 8.1 Hz, 1H), 7.93 (d, *J* = 8.7 Hz, 1H), 7.88 (d, *J* = 8.3 Hz, 1H), 7.62 (s, 3H), 4.59 (dd, *J* = 13.1, 7.7 Hz, 1H), 4.50 – 4.40 (m, 1H), 4.38 – 4.27 (m, 1H), 4.12 (dd, *J* = 13.7, 7.7 Hz, 1H), 2.80 – 2.70 (m, 3H), 1.44 (m, 12H), 0.83 (m, 12H). HRMS (ESI) $[M + Na]^+$ calculated: 961.5693, found: 961.5667, $[M + H]^+$ calculated: 939.5873, found: 939.5885, $[M + 2H]^{2+}$ calculated: 470.2973, found: 470.2986.

CP15: *Linear:* H-Asp(tBu)-D-Leu-Lys(Boc)-D-Leu-Asp(tBu)-D-Leu-Lys(Boc)-D-Leu-Asp(tBu)-D-Leu-Lys(Boc)-D-Leu-OH. White powder, 51.7% yield, MS-ESI (deprotected): $[M + H]^+$ 1428.30, $[M + 2H]^{2+}$ 714.60. *Cyclic: cyclo*[(Asp-D-Leu-Lys-D-Leu)$_3$]. Purification gradient: 20-60% buffer B over 60 min, R_T = 22.5 min (35.0% B). Yield: 5.8 mg (8.9%). ^{1}H NMR (400 MHz, DMSO-*d*$_6$) δ 12.38 (s, 1H), 8.28 (d, *J* = 4.0 Hz, 1H), 8.14 – 7.93 (m, 3H), 7.63 (s, 3H), 4.57 (dd, *J* = 13.6, 6.9 Hz, 1H), 4.39 – 4.26 (m, 3H), 2.79 – 2.55 (m, 5H), 1.73 – 1.37 (m, 11H), 1.30 – 1.20 (m, 2H), 0.90 – 0.79 (m, 12H). HRMS (ESI) $[M + H]^+$ calculated: 1408.8774, found: 1408.8768, $[M + 2H]^{2+}$ calculated: 704.9423, found: 704.9440, $[M + 3H]^{3+}$ calculated: 470.2973, found: 470.2988.

Crystallisation: Crystal screening was performed at the CSIRO C3 crystallisation centre using sitting drop vapour-diffusion in 96 well plates with droplets of 150 nL peptide and 150 nL of reservoir solution, equilibrated against a reservoir of 50 uL. Initial screens were set up using the 'shotgun' screen[27] at 20°C and each well was imaged by robot 15 times over a period of 80 days. Conditions that provided initial crystal hits were selected for further additive optimisation, using the Additive Screen HT (Hampton Research, USA) mixed with the original hit condition (90:10 v/v original condition:additive). Crystals were often seen after 1 day and grew to final size within 7 days. Peptides were found to crystallise best at concentrations of 5 mg/mL, as 10 mg/mL often caused precipitation and < 2 mg/mL provided little to no supersaturation (precipitation or crystal growth).

Crystallography: Diffraction data was collected using the MX2 micro-focus beamline at the Australian Synchrotron[20] on an ADSC Quantum 315r CCD detector for **2**, and a Dectris Eiger 16M for **8**, at 100(2) K using Si(111) monochromated synchrotron radiation. BluIce control software[28] was used for data-collection and integration was carried out with XDS.[29] Structure of CP **8** was solved by dual space methods using SHELXT[21] and refined with SHELXL.[22] The structure of CP **2** was solved by molecular replacement in the CCP4 suite[23] using Phaser[24] for initial model fitting, an initial refinement in Refmac,[25] and the final refinement with SHELXL.[22] Crystal data for **2** and **8** are given in **Table S2**. CCDC 2080714 (CP **2**) and 2085876 (CP **8**) contain the supplementary crystallographic data for this paper. These data are provided free of charge by the Cambridge Crystallographic Data Centre.

^{1}H-D exchange by NMR spectroscopy: ^{1}H-D exchange experiments were performed following our previously reported method.[6a] 1D ^{1}H NMR spectra of peptide products were recorded on a 600 MHz Bruker Avance III HD spectrometer with CryoProbe, at 298 K. Samples were dissolved in 100% D_2O for ^{1}H-D exchange experiments. The pH of samples was measured to be 3.0 ± 0.3. All of the NMR spectra were processed using TopSpin 3.0 (Bruker BioSpin GmbH). ^{1}H-D exchange studies were performed immediately following dissolution of CPs at 8 mM (CP **14** was dissolved at 4 mM due to poor solubility) in 100% D_2O. The first spectrum was acquired within 10 min of dissolution and up to 13 spectra in total were acquired over 60 to 90 min, depending on the rate of H^N signal exchange. CP half-lives were calculated from the decay over time of H^N proton signal integrals, relative to stable Leu methyl protons or $H^{C\alpha}$ proton signals. CP half-lives were averaged according to the number of unique backbone H^N signals (i.e., *cyclo*[(DłKł)$_2$] (CP **2**) has two-fold symmetry and thus four unique backbone H^N signals, while *cyclo*(DłKłKłKł) (CP **11**) has no symmetry and thus all eight backbone H^N signals are unique).

Turbidity assessment: Samples were assessed by eye for turbidity and ranked as low, medium or highly turbid samples. Examples of turbidity are provided in the supporting information (**Figure S14**).

Molecular Dynamics simulations: Model building and molecular dynamics studies were conducted in Maestro (Schrödinger version 10.3) using the integrated Desmond MD software (D. E. Shaw Research, version 4.3).[30] CP subunits were built manually using the crystal structure of CP **2**[9] as a backbone scaffold for antiparallel backbone-backbone hydrogen bonded dimers. Dimers were minimised in water for 2500 iterations using the OPLS 2005 forcefield[31] prior to preparation of the system for simulation. Systems were prepared as orthorhombic cells of 35 x 35 x 35 Å and were solvated with SPC water containing 0.15 M NaCl and additional Na^+/Cl^- counterions to neutralise the system. Simulations were conducted under the OPLS 2005 forcefield with NPT ensemble class at

300 K and 1.01325 bar with a 2 fs timestep. Nose-Hoover chain was employed for the thermostat method and Martyna-Tobias-Klein for the barostat method. Simulations used periodic boundary conditions and the particle-mesh Ewald method for long range electrostatics. Simulations were run for 100 ns and evaluated for stability according to the number of intermolecular backbone-backbone H-bonds.

Acknowledgements

MRS acknowledges an RTP scholarship provided by the Australian Government. BAL acknowledges support provided by the Norwegian Research Council (262695 and 274858). Initial crystal screening was performed at the CSIRO Collaborative Crystallisation Centre (www.csiro.au/C3), Melbourne, Australia. This research was undertaken in part using the MX2 beamline at the Australian Synchrotron, part of ANSTO, and made use of the Australian Cancer Research Foundation (ACRF) detector.

Keywords: cyclic peptides • nanotubes • self-assembly • molecular dynamics • X-ray crystallography

[1] aM. R. Ghadiri, J. R. Granja, R. A. Milligan, D. E. McRee, N. Khazanovich, *Nature* **1993**, *366*, 324-327; bM. R. Ghadiri, K. Kobayashi, J. R. Granja, R. K. Chadha, D. E. McRee, *Agew. Chem. Int. Ed.* **1995**, *34*, 93-95; cJ. D. Hartgerink, J. R. Granja, R. A. Milligan, M. R. Ghadiri, *J. Am. Chem. Soc.* **1996**, *118*, 43-50.

[2] aP. D. Santis, S. Morosetti, R. Rizzo, *Macromolecules* **1973**, *7*, 52-58; bL. Tomasic, G. P. Lorenzi, *Helvetica Chimica Acta* **1987**, *70*, 1012 - 1016.

[3] V. Pavone, Benedetti, Ettore, B. Di Blasio, A. Lombardi, C. Pedone, L. Tomasich, G. P. Lorenzi, *Biopolymers* **1989**, *28*, 215-223.

[4] R. Chapman, M. Danial, M. L. Koh, K. A. Jolliffe, S. Perrier, *Chemical Society reviews* **2012**, *41*, 6023-6041.

[5] aC. Steinem, A. Janshoff, M. S. Vollmer, M. R. Ghadiri, *Langmuir* **1999**, *15*, 3956-3964; bM. S. Vollmer, T. D. Clark, C. Steinem, M. R. Ghadiri, *Angew Chem Int Ed* **1999**, *38*, 1598-1601; cR. Gokhale, J. Couet, M. Biesalski, *Phys Status Solidi A* **2010**, *207*, 878-883; dJ. H. V. Maarseveen, W. S. Horne, M. R. Ghadiri, *Org. Lett.* **2005**, *7*, 4503-4506; eT. D. Clark, M. R. Ghadiri, *J. Am. Chem. Soc.* **1995**, *117*, 12364-12365; fT. D. Clark, K. Kobayashi, M. R. Ghadiri, *Chem-Eur J* **1999**, *5*, 782-792.

[6] aM. R. Silk, B. Mohanty, J. B. Sampson, M. J. Scanlon, P. E. Thompson, D. K. Chalmers, *Angewandte Chemie* **2019**, *58*, 596-601; bA. Fuertes, H. L. Ozores, M. Amorin, J. R. Granja, *Nanoscale* **2017**, *9*, 748-753; cH. L. Ozores, M. Amorin, J. R. Granja, *Journal of the American Chemical Society* **2017**.

[7] aM. Amorin, L. Castedo, J. R. Granja, *J. Am. Chem. Soc.* **2003**, *125*, 2844-2845; bM. Amorin, L. Castedo, J. R. Granja, *Chemistry* **2005**, *11*, 6543-6551; cD. T. Bong, M. R. Ghadiri, *Angewandte Chemie* **2001**, *40*, 2163-2166; dR. J. Brea, M. Amorin, L. Castedo, J. R. Granja, *Angewandte Chemie* **2005**, *44*, 5710-5713; eR. J. Brea, L. Castedo, J. R. Granja, *Chemical communications* **2007**, 3267-3269.

[8] M. Amorin, L. Castedo, J. R. Granja, *Chemistry* **2008**, *14*, 2100-2111.

[9] M. R. Silk, J. Newman, J. C. Ratcliffe, J. F. White, T. Caradoc-Davies, J. R. Price, S. Perrier, P. E. Thompson, D. K. Chalmers, *Chem Commun* **2017**, *53*, 6613-6616.

[10] aX. Sun, G. P. Lorenzi, *Helvetica Chimica Acta* **1994**, *77*, 1520-1526; bC. Reiriz, L. Castedo, J. R. Granja, *Journal of peptide science : an official publication of the European Peptide Society* **2008**, *14*, 241-249.

[11] aK. Kobayashi, J. R. Granja, M. R. Ghadiri, *Angewandte Chemie* **1995**, *34*, 95-98; bW. S. Horne, N. Ashkenasy, M. R. Ghadiri, *Chem. Eur. J.* **2005**, *11*, 1137-1144.

[12] aN. Rodriguez-Vazquez, R. Garcia-Fandino, M. J. Aldegunde, J. Brea, M. I. Loza, M. Amorin, J. R. Granja, *Organic letters* **2017**; bR. Hourani, C. Zhang, R. van der Weegen, L. Ruiz, C. Li, S. Keten, B. A. Helms, T. Xu, *Journal of the American Chemical Society* **2011**, *133*, 15296-15299.

[13] aD. Asthagiri, D. Bashford, *Biophysical journal* **2002**, *82*, 1176-1189; bH. Hwang, G. C. Schatz, M. A. Ratner, *J. Phys. Chem. B* **2006**, *110*, 6999-7008; cR. Garcia-Fandino, J. R. Granja, M. D'Abramo, M. Orozco, *J. Am. Chem. Soc.* **2009**, *131*, 15678-15686; dH. Liu, J. Chen, Q. Shen, W. Fu, W. Wu, *Molecular Pharmaceutics* **2010**, *7*, 1985-1994; eJ. Liu, J. Fan, M. Tang, M. Cen, J. Yan, Z. Liu, W. Zhou, *J. Phys. Chem. B* **2010**, *114*, 12183-12192; fR. Li, J. Fan, H. Li, X. Yan, Y. Yu, *The journal of physical chemistry. B* **2013**, *117*, 14916-14927; gJ. Montenegro, M. R. Ghadiri, J. R. Granja, *Accounts of Chemical Research* **2013**, *46*, 2955-2965; hM. A. Alsina, J. F. Gaillard, S. Keten, *Physical chemistry chemical physics : PCCP* **2016**, *18*, 31698-31710.

[14] R. Vijayaraj, S. S. Raman, R. M. Kumar, V. Subramanian, *J. Phys. Chem. B* **2010**, *114*, 16574-16583.

[15] R. Vijayaraj, S. Van Damme, P. Bultinck, V. Subramanian, *The journal of physical chemistry. B* **2012**, *116*, 9922-9933.

[16] R. Garcia-Fandino, L. Castedo, J. R. Granja, S. A. Vazquez, *J. Phys. Chem. B* **2010**, *114*, 4973-4983.

[17] J. Zhu, J. Cheng, Z. Liao, Z. Lai, B. Liu, *Journal of computer-aided molecular design* **2008**, *22*, 773-781.

[18] C. T. Mant, J. M. Kovacs, H.-M. Kim, D. D. Pollock, R. S. Hodges, *Biopolymers* **2009**, *92*, 573-595.

[19] V. J. Fazio, T. S. Peat, J. Newman, *Acta Crystallographica Section F* **2014**, *70*, 1303-1311.

[20] D. Aragao, J. Aishima, H. Cherukuvada, R. Clarken, M. Clift, N. P. Cowieson, D. J. Ericsson, C. L. Gee, S. Macedo, N. Mudie, S. Panjikar, J. R. Price, A. Riboldi-Tunnicliffe, R. Rostan, R. Williamson, T. T. Caradoc-Davies, *J Synchrotron Radiat* **2018**, *25*, 885-891.

[21] G. M. Sheldrick, *Acta Crystallographica Section A* **2015**, *71*, 3-8.

[22] G. M. Sheldrick, *Acta Crystallographica Section A* **2008**, *64*, 112-122.

[23] M. D. Winn, C. C. Ballard, K. D. Cowtan, E. J. Dodson, P. Emsley, P. R. Evans, R. M. Keegan, E. B. Krissinel, A. G. Leslie, A. McCoy, S. J. McNicholas, G. N. Murshudov, N. S. Pannu, E. A. Potterton, H. R. Powell, R. J. Read, A. Vagin, K. S. Wilson, *Acta Cryst.* **2011**, *D67*, 235-242.

[24] A. J. McCoy, R. W. Grosse-Kunstleve, P. D. Adams, M. D. Winn, L. C. Storoni, R. J. Read, *Journal of Applied Crystallography* **2007**, *40*, 658-674.

[25] G. N. Murshudov, A. A. Vagin, E. J. Dodson, *Acta Cryst.* **1997**, *D53*, 240-255.

[26] H. T. Kuo, C. J. Fang, H. Y. Tsai, M. F. Yang, H. C. Chang, S. L. Liu, L. H. Kuo, W. R. Wang, P. A. Yang, S. J. Huang, S. L. Huang, R. P. Cheng, *Biochemistry* **2013**, *52*, 9212-9222.

[27] V. J. Fazio, T. S. Peat, J. Newman, *Acta crystallographica. Section F, Structural biology communications* **2014**, *70*, 1303-1311.

[28] T. M. McPhillips, S. E. McPhillips, H. J. Chiu, A. E. Cohen, A. M. Deacon, P. J. Ellis, E. Garman, A. Gonzalez, N. K. Sauter, R. P. Phizackerley, S. M. Soltis, P. Kuhn, *Journal of Synchrotron Radiation* **2002**, *9*, 401-406.

[29] W. Kabsch, *J. Appl. Cryst.* **1993**, *26*, 795-800.

[30] K. J. Bowers, E. Chow, H. Xu, R. O. Dror, M. P. Eastwood, B. A. Gregersen, J. L. Klepeis, I. Kolossvary, M. A. Moraes, F. D. Sacerdoti, J. K. Salmon, Y. Shan, D. E. Shaw, *Proceedings of the ACM/IEEE Conference on Supercomputing (SC06), Tampa, Florida* **2006**.

[31] aW. L. Jorgensen, D. S. Maxwell, J. Tirado-Rives, *Journal of the American Chemical Society* **1996**, *118*, 11225-11236; bG. A. Kaminski, R. A. Friesner, J. Tirado-Rives, W. L. Jorgensen, *The Journal of Physical Chemistry B* **2001**, *105*, 6474-6487.

Entry for the Table of Contents

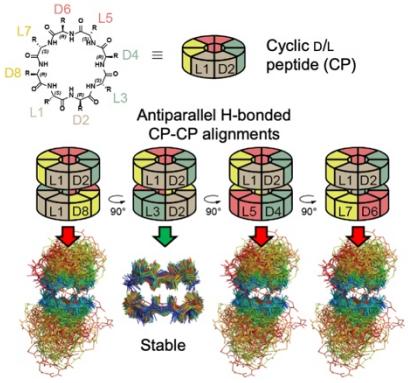

Cyclic D/L peptide nanotubes (CPNs) have diverse applications in biological and materials science. We study the impact of sidechain alignment, hydrophobicity and charge on CPN stability and report crystal structures of non-tubular folded peptide conformations. Molecular dynamics simulations correlate with measured H-bond half-lives, showing how the composition and relative orientation of amino acids are key factors in CPN stability.